International Forum on Aeroelasticity and Structural Dynamics
IFASD 2017
25-28 June 2017 Como, Italy

# STATIC FULLY COUPLED SIMULATION OF A TRANSPORT AIRCRAFT HIGH-LIFT SYSTEM

**Alessandro Lurgo**[1] **and Robert Jung**[2]

[1]IBK Technologie
Hamburg, Germany
alessandro.lurgo.external@airbus.com

[2]Airbus Germany
Airbus Allee 1, Bremen, Germany
robert.jung@airbus.com

**Keywords:** Aeroelasticity, Multibody, Co-simulation, Mesh deformation, Radial basis functions

**Abstract:** Whenever the structure of an aircraft component is significantly flexible, change in aerodynamic surfaces due to the structural flexibility must be taken into account in order to accurately model the behaviour of the component under aerodynamic load. This paper describes an industrial quasi steady aeroelastic application of an iteractive Computational Fluid Dynamics (CFD) - Computational Structure Mechanics (CSM) co-simulation approach. This kind of approach is expected to represent a substantial improvement in predicting loads on component level. In this paper the outboard flap system of a commercial aircraft is analysed. The model is built up with the commercial multibody software Adams. Particular care has been taken to model non-linear elements. The aerodynamic flow is modelled through steady non-linear Reynolds Averaged Navier-Stokes (RANS) equations, including the engine jet efflux on the outboard flap system. The flow field is solved using the DLR ('National Aeronautics and Space Centre') TAU code. A static analysis of the coupled system is presented. Towards the end of this paper, a test case for an unsteady Adams-TAU co-simulation of a wing is performed. The results are compared to a Nastran-Tau co-simulation of the same wing. This work represents a step towards the realization of an unsteady aeroelastic co-simulation of the outboard flap system using the multibody approach.

## 1 INTRODUCTION

The component analysed in this article the outboard flap system of a commercial aircraft. The purpose of the high-lift system is to increase the surface and the camber of the wing through the deployment of additional aerodynamic surfaces, the flap bodies. The deployment mechanisms are mounted in streamlined bodies called fairings bodies, Fig 1. The whole system is located at the wing trailing edge where, in addition to the aerodynamic load due to a particular flight condition, it may be subjected as well to the load generated by the engine jet efflux. Structural deformations due to aerodynamic load may change the aerodynamic load distribution, compared to the initial rigid configuration, which may result in significant changes to the aeroelastic behaviour of the component. In this context, there is a clear need to include fluid-structure interactions and consider engine jet efflux effects. This approach represents an improvement in studying such components. The co-simulation is performed in a multi-disciplinary environment on a parallel cluster architecture [4].

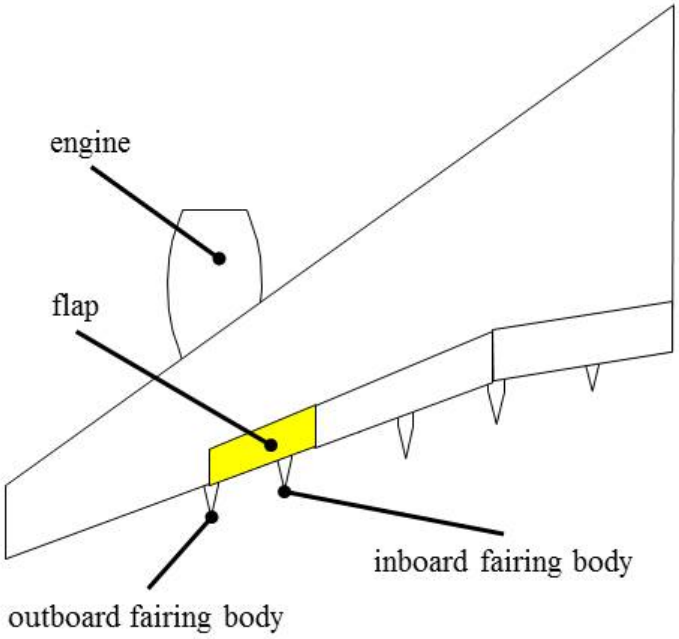


Figure 1: High-lift system of a commercial aircraft

## 2 OUTBOARD FLAP SYSTEM DESCRIPTION

The outboard flap system is comprised of two flap track stations and a flap body. In Fig. 2, an overview of the outboard flap system with the flap body and the deployment mechanisms of the inboard and outboard flap track stations is given. In Fig. 3, a schematic representation of one flap track station is shown. Each flap track station is further divided into: trackbeam, flap deployment mechanism, fairing kinematics and fairing body. The trackbeam connects the flap body and the flap deployment mechanism to the lower side of the wing through two attachment points. The flap deployment mechanism moves the flap body into position rotating a lever (rotary) and the motion is transferred to the flap body through the drive strut. The carriage slides on the top of the trackbeam while the rear link rotates. Each flap track station is enclosed by a fairing body in order to minimize the aerodynamic drag. During deployment of the flap body, the fairing body is moved by its own deployment mechanism (fairing kinematics) which is coupled with the flap deployment mechanism. The front connections, one on each side, of the fairing body to the trackbeam are called pivots. The second attachment point, the rear connection, located in the rear part of the fairing body, connects the faring body to the fairing kinematics. This joint configuration allows the faring to rotate during deployment and retraction of the flap body about the axis formed by the two pivots.

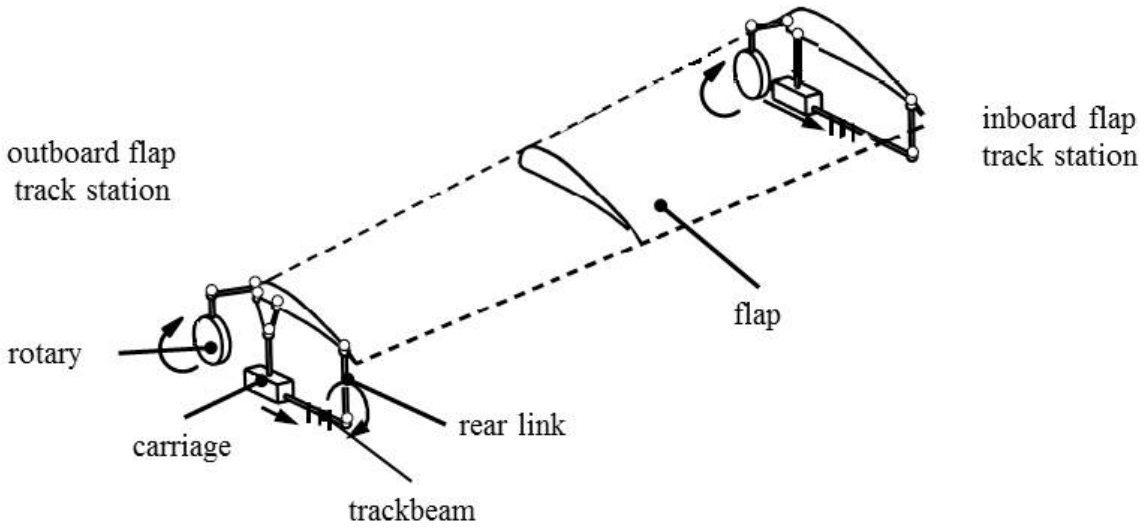


Figure 2: Outboard flap system. For more details about the Adams modeling, see [8]

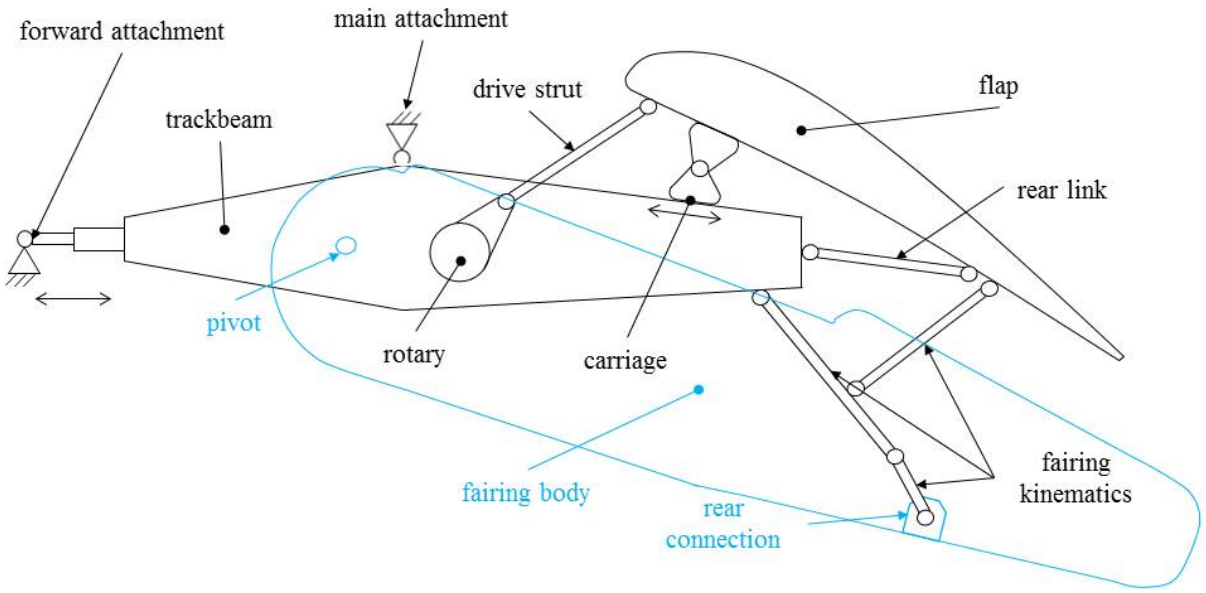


Figure 3: Flap track station

### 2.1 Attachment points

The two trackbeams support the weight of the outboard flap system and transfer the loads acting on flap body and fairing bodies to the wing through two connection points per trackbeam: forward attachment point and main attachment point. This design is chosen in order to embed the very stiff trackbeam into the deformable wing structure. The main attachment point comprises a spigot and two friction pads, Fig. 4. The spigot works like a bolt which is connected to the structure of the wing. The connection to the wing allows the spigot to rotate three-dimensionally. The connection from the spigot to the trackbeam allows the trackbeam to rotate around the spigot axis. The spigot is preloaded by tightening a screw nut in order to sustain the weight of the flap track station and to compress the pads. The pads are friction elements that generate friction forces through compression. The function of the friction pads is two-fold: they prevent the rotation of the trackbeam around the line connecting the two attachment points, and they counteract the rotation of the trackbeam around the spigot axis. This particular design, where a proper joint is substituted through two friction elements, introduces nonlinearities into the structural model. Details of the main attachment point and its multibody modeling are explained in Sec. 3. The forward attachment point also comprises a spigot but no friction elements and preload are present. The forward connection to the wing structure allows the trackbeam to translate along the spigot axis and rotate about the connection between spigot and wing structure.

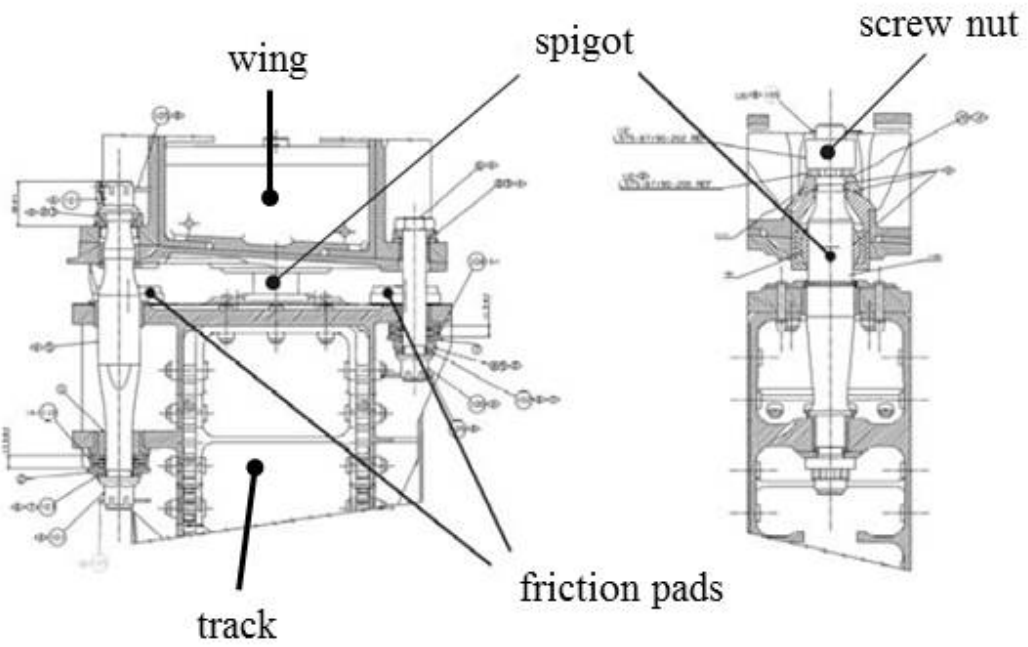


Figure 4: Main attachment point detail: spigot and friction pads

## 3 STRUCTURAL MODELING

The modeling of the outboard flap system is represented with the multibody software Adams. The model comprises rigid bodies as well as flexible bodies connected with ideal joints. The

flap deployment mechanism parts (rotary, drive strut, carriage and rear link) and the fairing kinematics are modelled as rigid body. The trackbeams, fairing bodies and flap body are considered as flexible bodies. One of the important features of the multibody model is the representation of the friction pads through contact forces. This choice enables the modeling of the friction forces introduced by the the friction pads, as descfibed in Subsec. 3.2.

### 3.1 Flexible bodies

Finite Element Models (FEM) of these components have been dynamically reduced through the Craig-Bampton reduction method. This method is implemented in Nastran and allows the representation of a flexible body through a reduced modal base and a set of boundary modes, whose scope is to capture the effects of the attachments. These two sets of modes are then mixed through an orthogonalization process and form the Craig-Bampton modal basis. Further details about this method can be found, for example, in the chapter "Component-Mode Synthesis" in [2]. Modal Neutral Files (mnf), used by Adams after mode reduction (see [5]) contain information about mass and stiffness matrices, as well as modal base and modal load of the flexible body. The flap body is modelled as beam model in Nastran. A representation of a cross section of the flap body is shown in Fig. 5 a, whereas, the model of the whole flap body is depicted in Fig. 5 b. The beam is located at the shear center of the flap body and rigid elements connect the beam with nose point, trailing edge and center of mass represented by a concentrated mass element. The flap body is connected with the deployment mechanisms of the inboard and outboard flap track stations through rigid bodies, called flap connections. The two trackbeams are modelled as beam model in Nastran. The beam is located at the center of mass of a trackbeam. Different sections of the beam are represented by beam elements with different area properties. The mass is represented as concentrated mass elements. A representation of the Adams modeling of one flap track station is given in Fig. 6. Regarding the inboard fairing, a detailed Nastran model is not available, therefore, it is also represented in Nastran with a beam model. As for the trackbeams, the beam is located at the center of mass. Beam elements with different area properties represent the different sections of the inboard fairing body and the mass is represented as concentrated mass elements. The outboard fairing is represented in Nastran with a detailed FEM consisting of beam elements, 2-D shell elements, and 3-D solid elements. In Fig. 7 the assembled Adams model of the outboard flap system is shown.

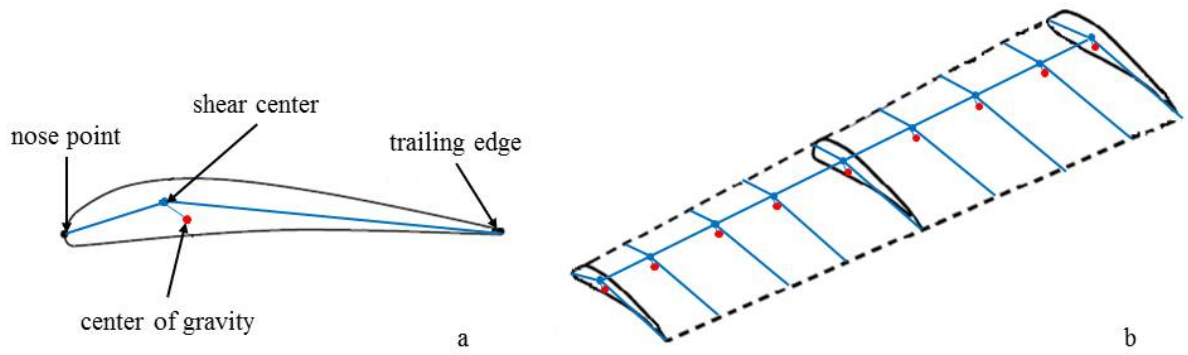


Figure 5: Outboard flap system modeling

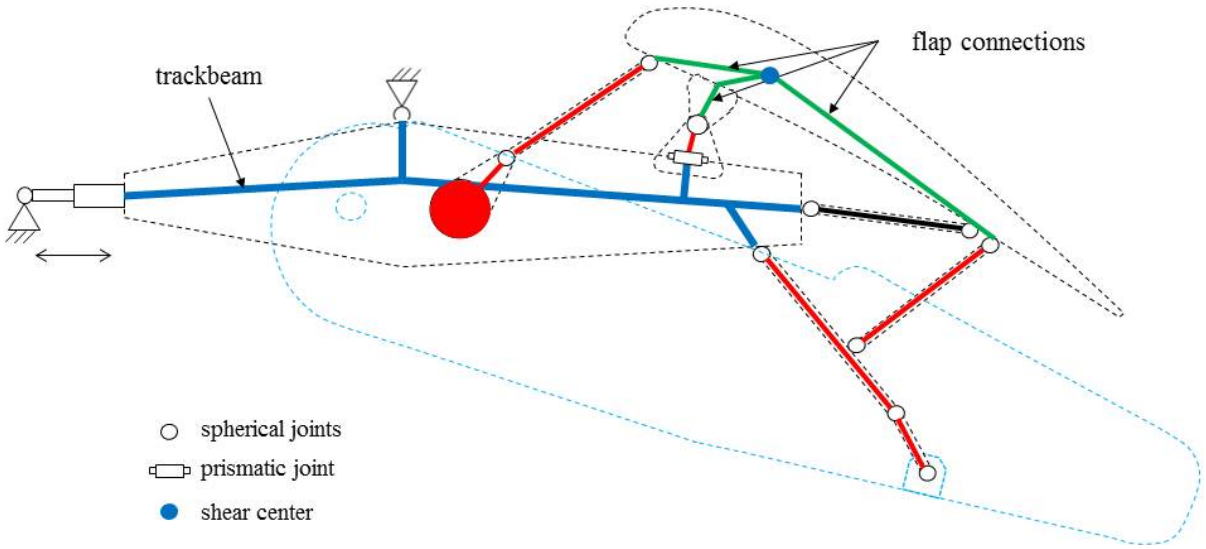


Figure 6: Station modeling

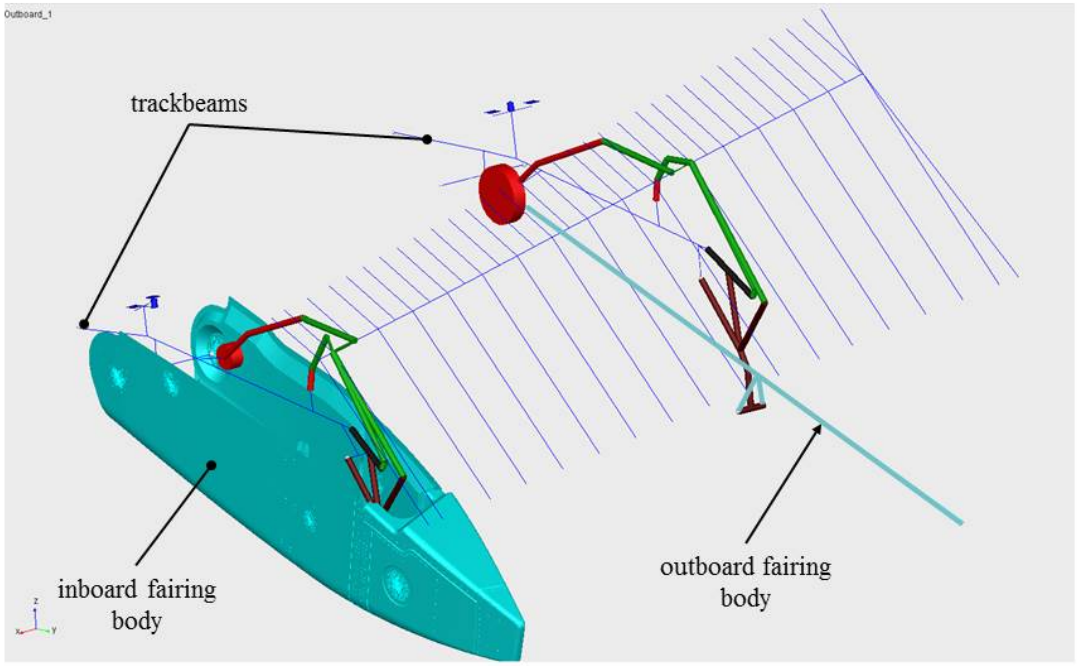


Figure 7: Adams outboard flap system model

### 3.2 Attachment points to the wing structure

In this subsection the approach adopted in the modeling of the attachment points is introduced. The forward connection of the trackbeam body to the wing structure is modelled with a spherical joint and a prismatic joint. Regarding the main attachment point, the connection wing structure-spigot is modelled with a spherical joint, whereas the connection spigot-trackbeam body is modelled with a cylindrical joint. The two friction pads that are represented in Adams by contact forces. A viscoelastic force normal to the pad surface, $F_{\text{pad}}$, with stiffness $k_{\text{pad}}$ and damping coefficient $c_{\text{pad}}$, is function of the compression length $d_{\text{pad}}$, and compression velocity $\dot{d}_{\text{pad}}$, as described in Eq. (1)

$$F_{\text{pad}} = \begin{cases} 0 & \text{if } d_{\text{pad}} > 0 \\ -k_{\text{pad}}\, d^{e}_{\text{pad}} - c_{\text{pad}}\, \dot{d}_{\text{pad}} & \text{if } d_{\text{pad}} \leq 0 \end{cases} \tag{1}$$

Adams contact force modellig allows the introduction of a friction force. An approximate model to describe a friction force is the Coulomb's representation, Eq. (2). In this model two friction states are distinguished: sticking and sliding. The first one occurs when the relative velocity between two bodies is zero, the latter when the relative velocity is different from zero. These two regimes are related to a static friction coefficient $\mu_s$ and a dynamic friction coefficient $\mu_d$. In the Coulomb model the transition between them is discontinuous.

$$\begin{cases} \vec{F}_{\text{friction}} \leq \mu_s\, F_{\text{pad}} & \text{if } |\vec{v}_{\text{rel}}| = 0 \\ \vec{F}_{\text{friction}} = \mu_d\, F_{\text{pad}}\, \frac{\vec{v}_{rel}}{|\vec{v}_{rel}|} & \text{if } |\vec{v}_{\text{rel}}| \neq 0 \end{cases} \tag{2}$$

Adams represents friction force in a regularized version of the Coulomb model: the transition between the static and kinematic friction is continuous, and the relative velocity is not required to be exactly zero, approximating the model of static friction (Fig. 8). For more details see [3] and [6].

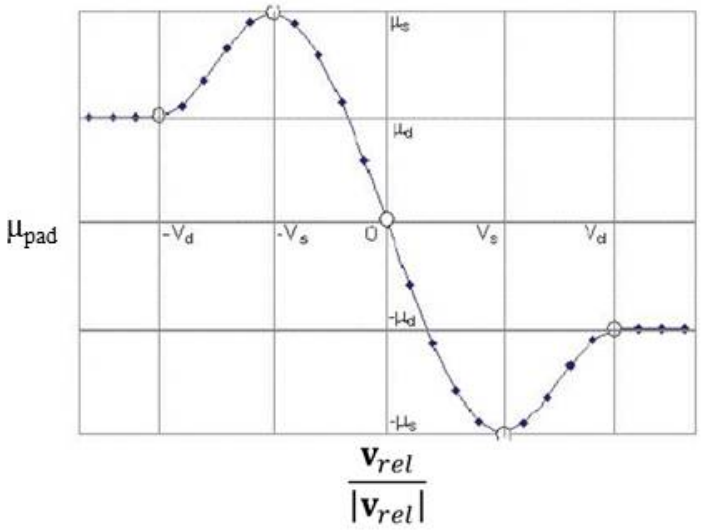


Figure 8: Adams friction coefficient vs. relative velocity

## 4 STATIC VALIDATION OF THE ADAMS MODEL

Two types of static validations have been performed:

1. Static validation of the Craig-Bampton modal bases of the flexible bodies
2. Static validation of the two flap track stations against Nastran model

### 4.1 Static validation of the Craig-Bampton modal bases of the flexible bodies

This subsection is dedicated to statically validate the Craig-Bampton modal bases of the flexible bodies resulting from the application of the Craig-Bampton reduction method. In Adams, each individual flexible body alone has been fixed to the ground and loaded with a static force of 1000 N in the direction of the trisectrix of the first quadrant of the cartesian plane. The deformations at the force application points, $\mathbf{d}_{Adams}$, are measured and compared with the deformations resulting from Nastran simulations, $\mathbf{d}_{Nastran}$. Outboard fairing has been fixed to the ground at the pivot locations and the static force applied at the tip of the tail cone, Fig 9. Inboard and outboard trackbeams have been fixed to the ground at the forward attachment location and the static force applied at the tip. The flap body is fixed to the ground at the the locations of the connections with the inboard and outboard flap track stations and the static force applied at a location of the trailing edge. In Nastan models, the same boundary conditions and load configurations have been replicated. The percentage ratio $\Delta d_{\%}$ is defined as

$$\Delta d_{\%} = \frac{|\mathbf{d}_{Nastran}| - |\mathbf{d}_{Adams}|}{|\mathbf{d}_{Nastran}|} * 100. \tag{3}$$

The results reported in Table. 1 show good agreement between Adams and Nastran for all the flexible bodies.

| Component | $\Delta d_{\%}$ |
|---|---|
| Inboard Track | -0.13 |
| Outboard Track | 0.0 |
| Outboard Flap | 0.0 |
| Outboard fairing | -2.4 |

Table 1: Static validation of the Craig-Bampton modal bases of the flexible bodies

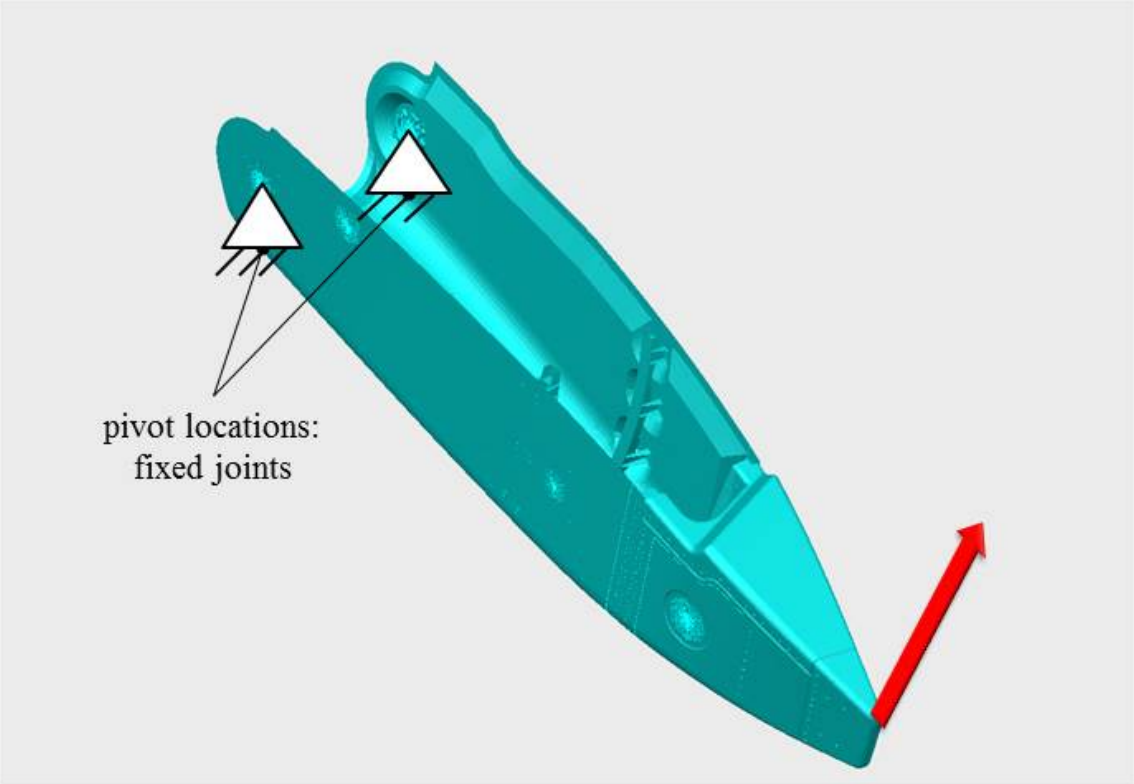


Figure 9: Static validation of the Craig-Bampton modal base of the outboard fairing

### 4.2 Inboard and outboard flap track stations static validation

The individual Adams models of inboard and outboard flap track stations have been statically verified against Nastran models. Adams joint forces at forward attachment point and at the elements of the main attachment point (spigot, inboard pad and outboard pad) have been compared with Nastran constrain forces. Each flap track station is loaded with a static force of 1000 N in the direction of the trisectrix of the first quadrante of the cartesian plane (red arrow in Fig. 10). Spigot preloads and gravity are considered. $\mathbf{F}_{Adams}$ and $\mathbf{F}_{Nastran}$ identify the constraint forces at each attachment element for both simulations. The percentage force ration $\Delta F_{\%}$ is defined as

$$\Delta F_{\%} = \frac{|\mathbf{F}_{Nastran}| - |\mathbf{F}_{Adams}|}{|\mathbf{F}_{Nastran}|} * 100. \tag{4}$$

The angles $\theta$ between Adams and Nastran constrain forces are also calculated. The results are reported in Table. 2 and Table. 3. A good overall correlation can be seen between Adams and Nastran force magnitudes and angles. The biggest differences in magnitude and angle are in the forward attachment point of the inboard flap track station and in the spigot of the outboard flap track station. Both friction pads take charge of most of the load on the flap track stations. Consequently, a small difference in orientation of Adams joint forces respect to Nastran constrain forces on the friction pads, results in big differences on spigot and forward attachment point. Reducing the preload on the spigots, Adams results show almost a perfect correlation with Nastran results.

| Component | $\Delta F_{\%}$ | $\theta$ [deg] |
|---|---|---|
| Spigot | -0.3 | 0.2 |
| Inboard Pad | 0.0 | 0.0 |
| Outboard Pad | 0.0 | 0.0 |
| Forward Attach | 6.5 | 2.1 |

Table 2: Force percentage ratios and angles for the inboard station

| Component | $\Delta F_{\%}$ | $\theta$ [deg] |
|---|---|---|
| Spigot | 5.2 | 10.3 |
| Inboard Pad | -0.1 | 2.9 |
| Outboard Pad | -0.1 | 2.9 |
| Forward Attach | -0.5 | 0.7 |

Table 3: Force percentage ratios and angles for the outboard station

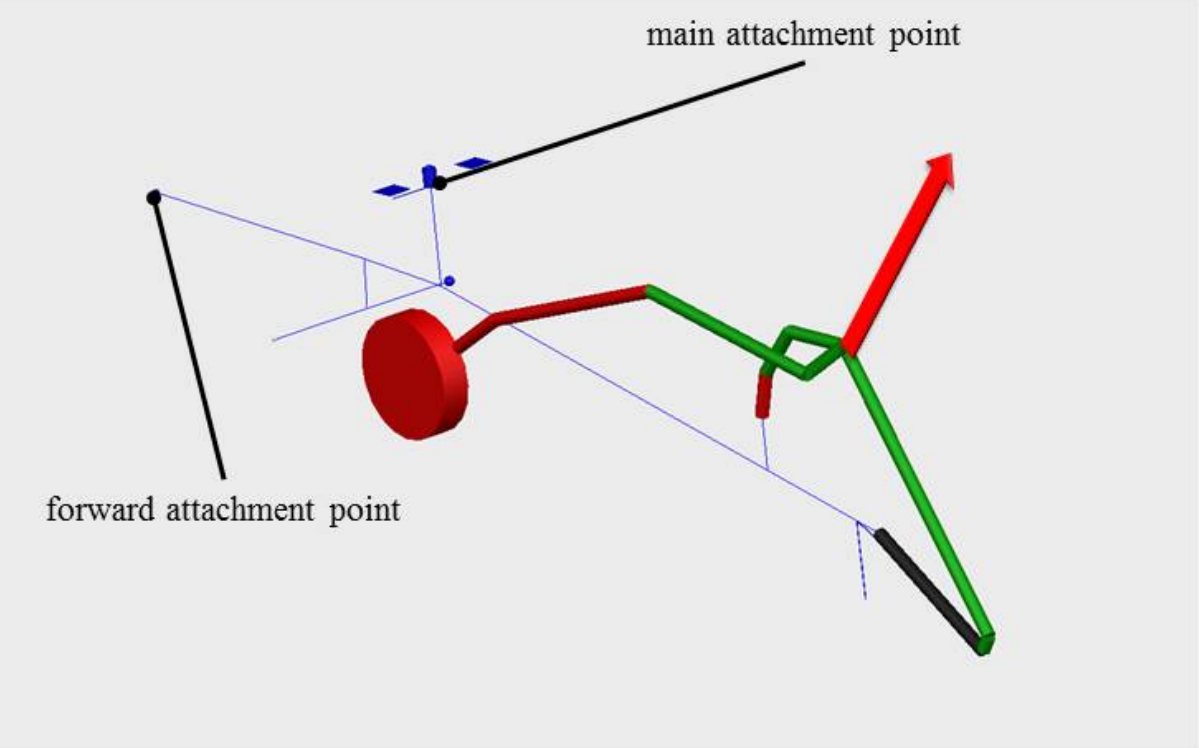


Figure 10: Static validation of inboard and outboard flap track stations

## 5 AERODYNAMIC MODELING

The complete aerodynamic mesh of the aircraft has been reduced to the outer section of the wing assembly, including engine and far-field beyond the tip of the wing. The decision of reducing the aerodynamic mesh has been taken into account with the scope of reducing the CFD computational cost while capturing the effect of the engine jet efflux on the neighbouring fairing. The equations solved are the steady Reynolds Averaged Navier-Stokes equations of motion with the Menter Shear Stress Transportation (Menter SST) two-equation turbulence model. For more details about the derivitation of the RANS equations and about various turbulence models see [7].

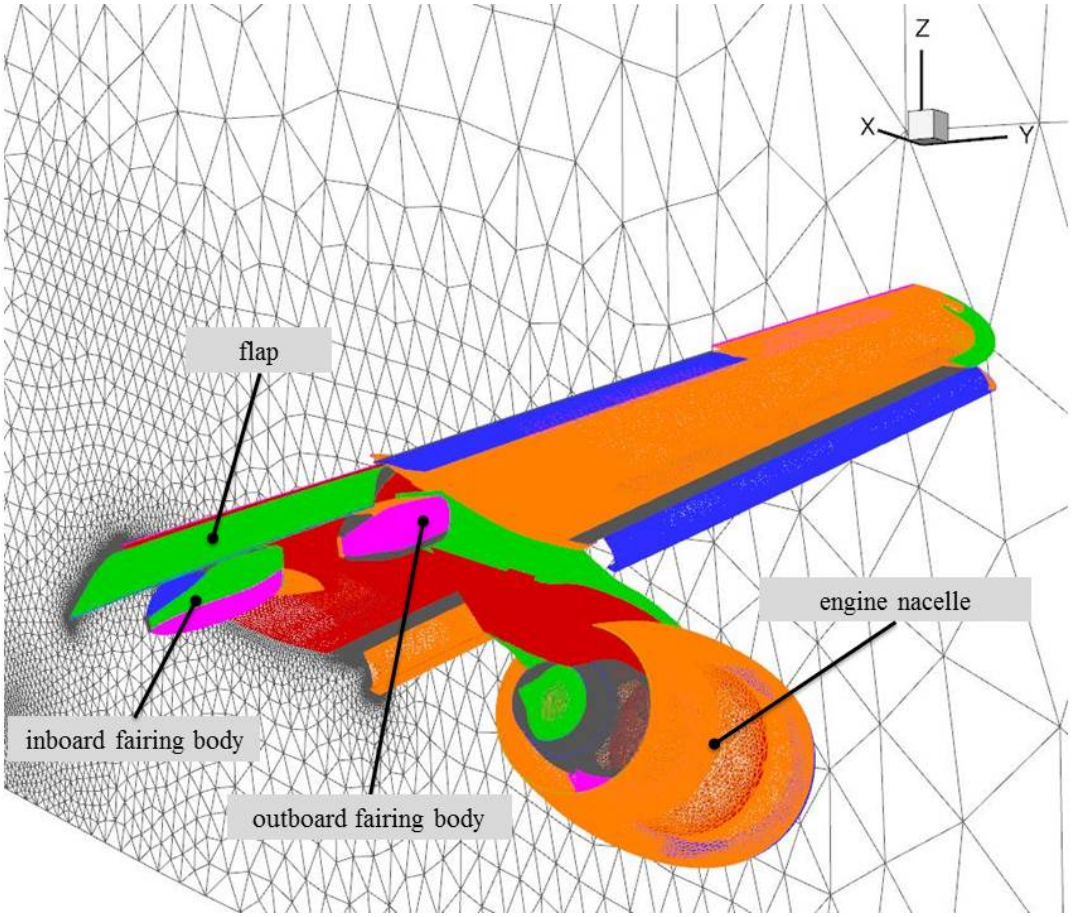


Figure 11: CFD Mesh of the outboard flap system

## 6 COUPLING PROCEDURE

The coupling process is performed with the Airbus in-house multi-disciplinary coupling environment [4], which controls the information exchange between the CFD and CSM model. A typical coupling iteration step is depicted in Fig. 12 and performed as follows: the aerodynamic solver calculates the aerodynamic pressures which are converted into forces on structural grids. Structural displacements $\mathbf{u}_s$ are then calculated by the structural solver and interpolated on the aerodynamic nodes $\mathbf{u}_f$ resulting in aerodynamic mesh update, Fig. 13. This iterative process continues until convergence is reached. Force transfer from CFD mesh to CSM grid is performed through a Nearest Neighbour Search (NNS) algorithm while CFD mesh deformation, due to structural deformation, is derived using radial basis function (RBF) interpolation, see

Sec. 6.1 and [1] for more details. These two tasks are performed within the multi-disciplinary coupling environment. A dedicated Python routine has been created to enable the communication between this environment and Adams.

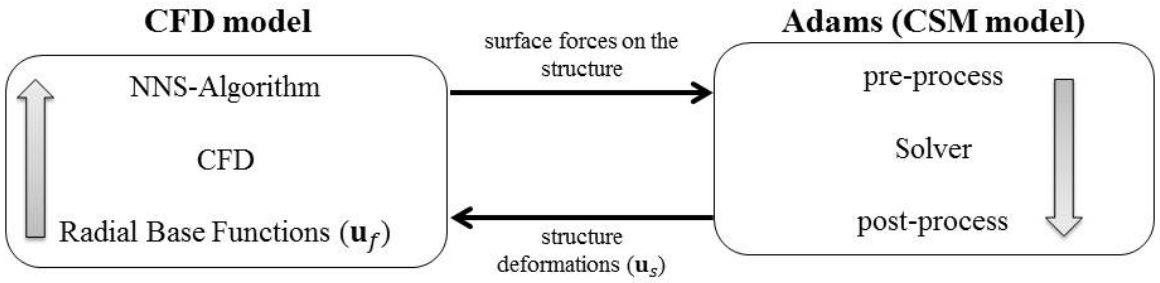


Figure 12: Coupling strategy

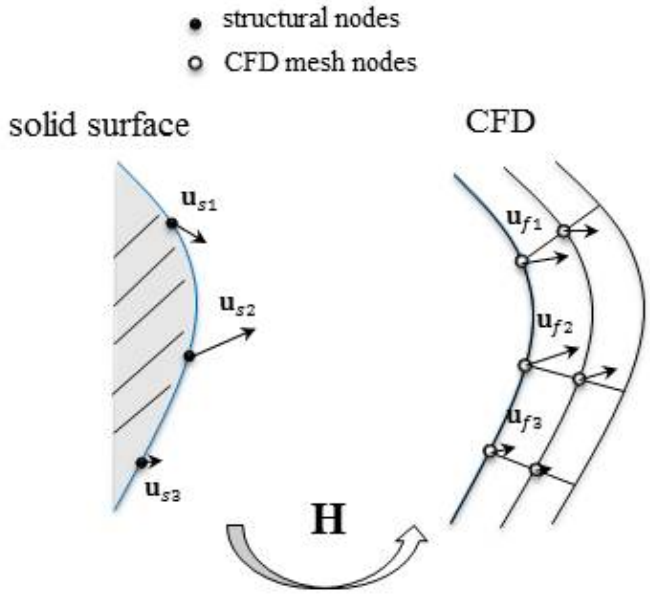


Figure 13: Structural displacements interpolation and mesh deformation

### 6.1 Radial Basis Function (RBF) interpolation for CFD mesh deformation

A function is a radial basis function when it has as argument only the distance $\|\mathbf{x} - \mathbf{x}_0\|$ from its origin $\|\mathbf{x}_0\|$

$$\phi = \phi(\|\mathbf{x} - \mathbf{x}_0\|). \tag{5}$$

A typical radial base function used in CFD-CSM co-simulations is shown in Fig. 14, its origin is $\mathbf{x}_0 = \mathbf{0}$. In CFD-CSM this type of functions can be used to interpolate the known structural displacement field $\mathbf{u}_s$ and to derive the unknown deformations of the aerodynamic nodes $\mathbf{u}_f$ as a linear approximation

$$\mathbf{u}_f = \mathbf{H}\,\mathbf{u}_s, \tag{6}$$

where the matrix $\mathbf{H}$ is the coupling interpolation matrix. For more details about radial base functions and the generation of the coupling interpolation matrix $\mathbf{H}$, see [1] and references therein.

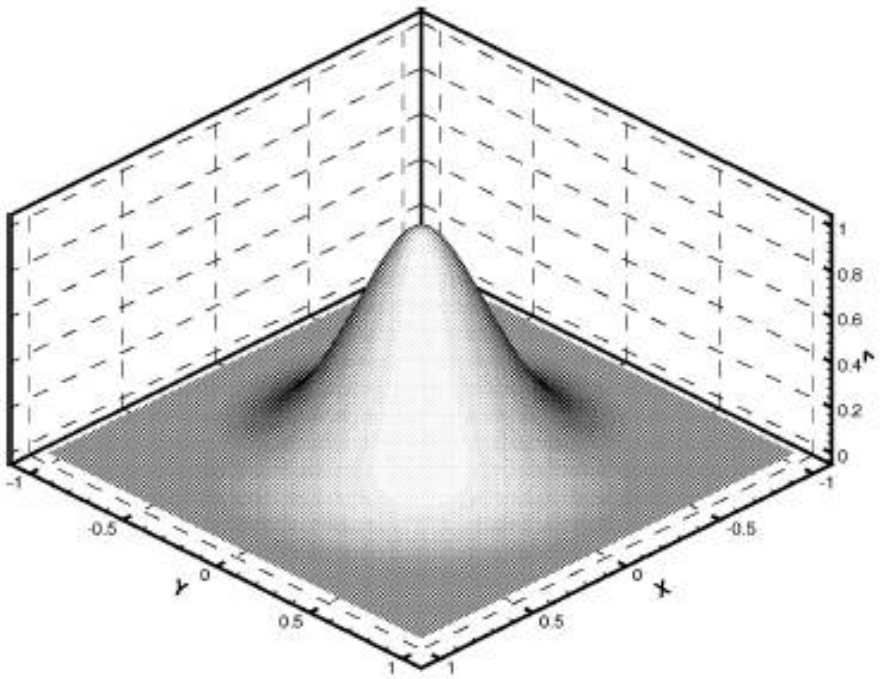


Figure 14: Typical radial base function used in CFD-CSM co-simulations

## 7 SIMULATION AND RESULTS

The outboard flap system is analysed in landing configuration. For each iteration, only the aerodynamic surfaces of outboard fairing body and flap body are updated in the coupling process. The focus of this study is the outboard faring body which is located behind the outer engine and it is directly influenced by the jet efflux. Some of the landing key parameters are presented in Table. 4.

| Parameter | Value |
|---|---|
| Mach nr. | 0.28 |
| Reynolds nr. | 80 Mil. |
| Air temperature [K] | 288.15 |

Table 4: Landing parameters

### 7.1 Static coupling simulation

In this section the result of a static CFD-Adams co-simulation is presented. The co-simulation has converged. In Fig. 15 and Fig. 16, the final deformations of the outboard flap system are shown. In particular, in Fig. 15 the outboard flap system is viewed from the outboard side, whereas in Fig. 16 the outboard flap system is viewed from the inboard side. The highest deformation values for the outboard fairing body are found on its lateral walls. Furthermore, it can be notices how the deformations are not symmetrical. This expected behaviour is due to the influence of the jet engine on the outboard fairing body, which is exciting the lateral structure of the outboard fairing body with a not symmetrical pressure field.

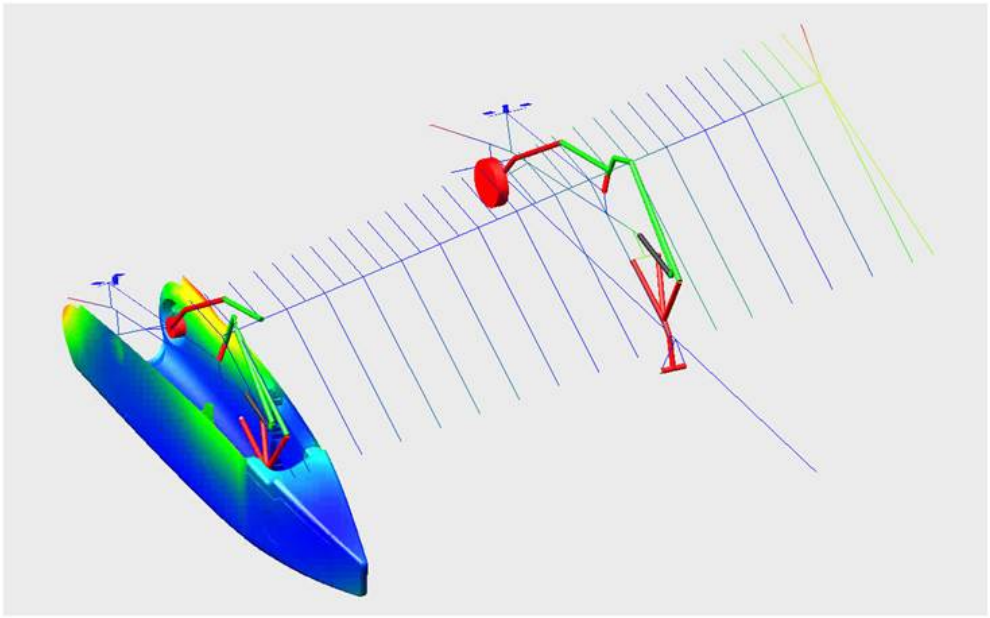

Figure 15: Deformations of the outboard flap system: outboard view.

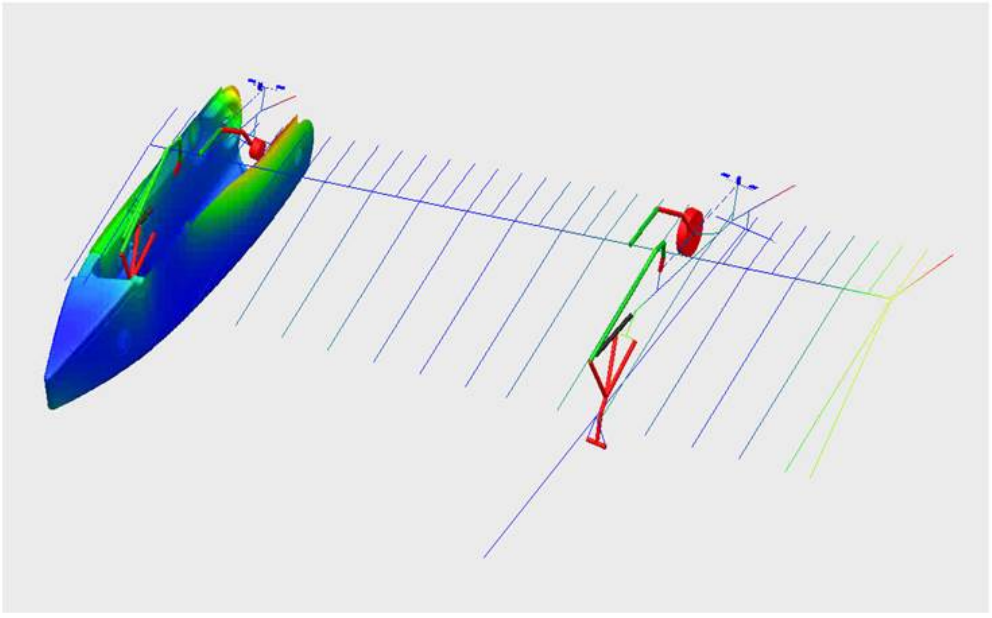

Figure 16: Deformations of the outboard flap system: inboard view.

## 8 UNSTEADY COUPLED SIMULATION OF THE LANN WING

In this section an unsteady CFD-CSM co-simualtion for the LANN wing is presented. The LANN wing was the result of a joint effort between Lockheed, the US Air Force, NASA and the Netherlands to measure unsteady pressures at transonic speeds. It has a moderate-aspect-ratio transport configuration and some details of its geometry are reported in Fig. 17. In the contest of this paper, the LANN wing has been used as a simplified test case for a Adams-Tau unsteady co-simulation.

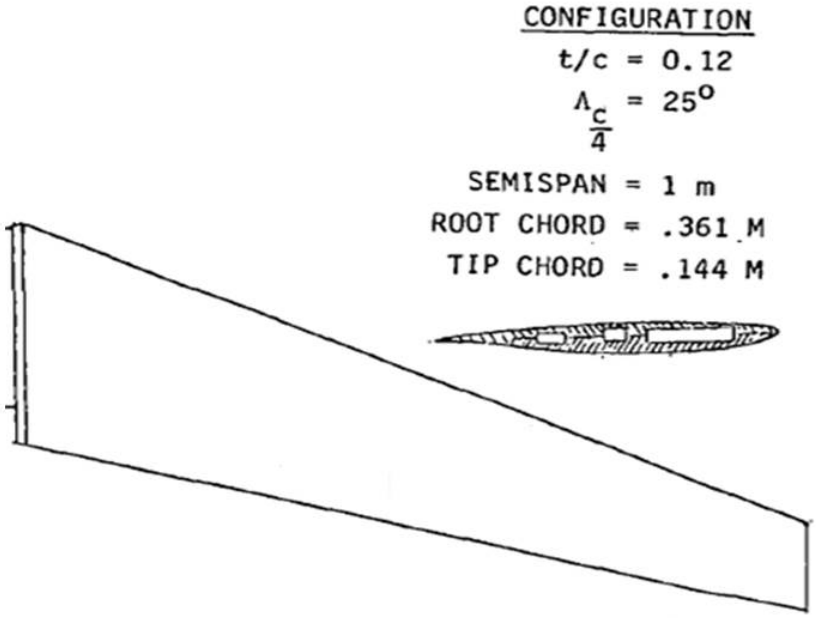


Figure 17: LANN wing specifications

### 8.1 Simulation

The LANN wing is represented as a cantilever beam, with the root fixed rigidly to the ground. Only the first two modes are considered in the calculation. The flowfield is represented with the Euler equations. The unsteady simulation is initiated with an initial modal displacements for the two generalized modal coordinates $q_1(t)$ and $q_2(t)$. In Table 5, frequencies and intial values for the two modes are reported. No modal damping is considered and some parameters of the unsteady simulation are shown in Table 6.

| Mode | Frequency [Hz] | Initial conditions at $t = 0$ |
|---|---|---|
| $q_1$ | 100.7 | 0.02 |
| $q_2$ | 233.4 | 0.02 |

Table 5: Frequencies and initial conditions for the generalized modal coordinates

| Parameter | Adams | Nastran |
|---|---|---|
| Time step size [s] | 0.0002 | 0.0004 |
| Number of time steps | 100 | 200 |
| Total simulation time [s] | 0.04 | 0.04 |

Table 6: Unsteady simulation parameters for the Adams-Tau and Nastran-Tau co-simulation

Results of an Adams-Tau co-simulation are compared to a Nastran-Tau co-simulation. The comparisons are shown in Fig. 18 for lift coefficient, maximal deformation, moment coefficient, $q_1(t)$ and $q_2(t)$. An overall good correlation between Adams and Nastran results can be seen for the analysed quantities. A light phase shift and numerical damping can be seen in $q_2(t)$ for the Nastran co-simulation respect to the Adams co-simulation.

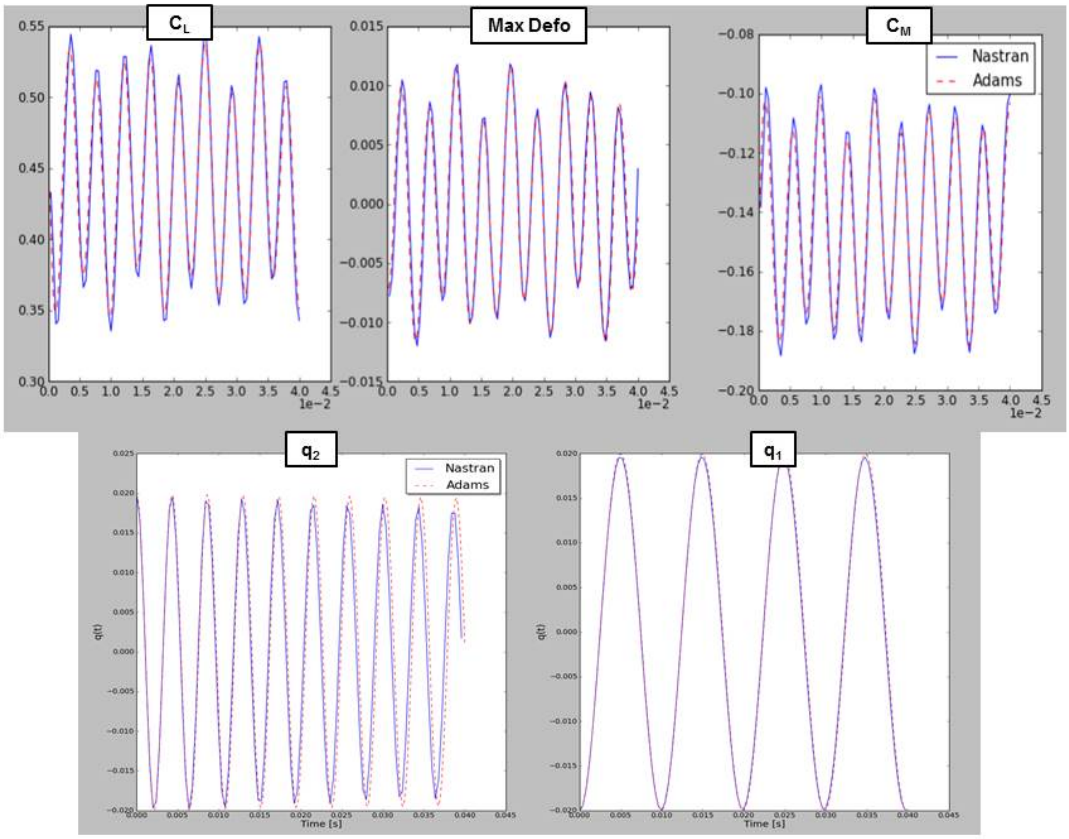


Figure 18: Unsteady results comparison between Adams-Tau and Nastran-Tau co-simulations.

## 9 CONCLUSIONS AND OUTLOOK

The presented work describes a fully coupled CFD-CSM co-simulation process, where change in aerodynamics surfaces due to structural deformation and engine jet efflux influence have been taken into account. These effects are significant for high-lift systems which are comprised of relatively flexible bodies compared to the external aerodynamic excitation. The results presented in subsection 7.1 show that the outboard fairing experiences not symmetrical deformations. These deformations influence the aerodynamic flow around the fairing body at every iteration step. This behaviour has particular importance in predicting the influence of engine jet efflux, which confirms the importance of considering structural deformations to capture change in aerodynamic flow for accurate load predictions. Furthermore, multibody approach modeling for high-lift systems allows:

1. modeling of rigid (kinematics) as well as flexible bodies (flaps, fairing bodies, ...)
2. a single model to represent different high-lift configurations (take off, landing, cruise),
3. modeling of non linearities (contact elements, joint friction, backlashes).

The status of the model and coupling routines has been proven to be robust in both steady and unsteady cases. Steady co-simulation of the outboard flap system represents the first step of this study. The setup of an unsteady co-simulation for the LANN wing presented in Sec. 8 represents an intermediate step, where the final aim is to reproduce the behaviour of the outboard flap system in the time domain. In this context, the Adams model will be dynamically validated against available ground test results and time domain coupling will be compared to the available flight test data.

## 10 REFERENCES

[1] Beckert A. and Wendland H.., *Multivariative interpolation for fluid-structure-interaction problems using radial basis functions*, Aerosp. Sci. Technol., 2001

[2] Craig Roy R., Fundamental of Structural Dynamics, Wiley, 2006

[3] Giesbers J., *Contact mechanics in MSC Adams*, Bachelor Thesis: Faculty of Engineering Technology University of Twente

[4] Meinel M. and Einarsson G., *The FlowSimulator framework for massively parallel CFD applications*, PARA 2010 conference 2010

[5] MSC.Software, *Using the Adams/Flex*, MechanicalDynamics Inc, Ann Arbor, MIchigan, 2002

[6] MSC.Software, *Using the Adams/View*, MechanicalDynamics Inc, Ann Arbor, MIchigan, 2002

[7] Wilcox David C., Turbulence Modeling for CFD, DCW Industries, 2004

[8] Zierath J., Woernle C., Heyden T, *Elastic multibody models of transport aircraft high-lift mechanisms*, AAIA J. Aircraft 46, 2009

## COPYRIGHT STATEMENT